Combustion and Flame 205 (2019) 41–54

Contents lists available at ScienceDirect

Combustion and Flame

journal homepage: www.elsevier.com/locate/combustflame

A species-clustered splitting scheme for the integration of large-scale chemical kinetics using detailed mechanisms

Jian-Hang Wang, Shucheng Pan*, Xiangyu Y. Hu*, Nikolaus A. Adams

Chair of Aerodynamics and Fluid Mechanics, Department of Mechanical Engineering, Technical University of Munich, Garching 85748, Germany

ARTICLE INFO

Article history:
Received 9 November 2018
Revised 21 January 2019
Accepted 25 March 2019
Available online 4 April 2019

Keywords:
Ordinary differential equations
Implicit solver
Detailed kinetic mechanisms
Operator splitting
Balanced clustering
n-heptane/n-hexadecane ignition

ABSTRACT

In this study, a species-clustered integrator for chemical kinetics with large detailed mechanisms based on operator-splitting is presented. The ordinary differential equation (ODE) system of large-scale chemical kinetics is split into clusters of species by using graph partition methods which have been intensely studied in areas of model reduction, parameterization and coarse-graining, e.g., diffusion maps based on the concept of Markov random walk. The definition of the weight (similarity) matrix is application-dependent and follows from chemical kinetics. Each species cluster is integrated by the variable-coefficient ODE solver VODE. The theoretically expected speedup in computational efficiency is reproduced by numerical experiments on three zero-dimensional (0D) auto-ignition problems, considering detailed hydrocarbon/air combustion mechanisms at varying scales, from 53 species with 325 reactions of methane to 2115 species with 8157 reactions of n-hexadecane. Optimal clustering weighing both prediction accuracy (for ignition delay and equilibrium temperature) and computational efficiency is implied with the clustering number $N = 2$ for the 53-species methane mechanism, $N = 4$ for the 561-species n-heptane mechanism and $N = 8$ for the 2115-species n-hexadecane mechanism.

1. Introduction

Gasoline, diesel and jet fuels, particularly those derived from petroleum sources, are composed of hundreds of components [1]. As the number of hydrocarbon species grows, so does the dimensionality of kinetic mechanism to model hydrocarbon oxidation. For example, the detailed mechanism for methyl decanoate, a biomass fuel surrogate, consists of 3036 species and 8555 reactions [2,3]. For the accurate prediction of combustion processes such as ignition, extinction and flame propagation, the efficient solution of large-scale detailed chemical kinetics is a key [4], limited, however, by the current computing power. The above-mentioned mechanism is time consuming even for 0D simulations [3], no matter whether using explicit or implicit solvers. This limitation therefore motivates to the development of mechanism reduction methods, e.g., directed relation graph (DRG) based methods [5–8], etc.

Moreover, numerical stiffness due to large differences of reaction timescales exists, so that the high-cost implicit ODE solvers, e.g., VODE [9] and DASAC [10], requires robust use of reasonably large timesteps [4]. Since Jacobian evaluation and factorization in implicit solvers dominate the computational cost for compressible and reactive CFD [11], the CPU time scales with the number of species in the mechanism as $\mathcal{O}(N^2)$ to $\mathcal{O}(N^3)$ with dense matrix operations [12,13].

For general multi-dimensional reactive flows, operator splitting has been widely used to separate chemistry integration from that of transport processes to reduce computational efforts [14–18]. Xu et al. [4] and Gao et al. [19] adaptively separate the dynamic system into a fast operator including only fast reactions and a slow operator including slow reactions and the transport process, with each part being imposed of an implicit solver and a more efficient explicit solver, respectively. For the chemical dynamics only, Nguyen et al. [20] aiming at preserving mass conservation and positivity solves each chemical reaction after splitting the multi-reaction system into decoupled processes. Pan *et al.* [21] introduce the graph/network partition into large-scale stochastic and mass concentration based chemical networks.

The quadric/cubic scaling of CPU time to mechanism size using implicit ODE solvers implies that the computational cost of solving a sequence of smaller subsystems ought to be much less than that of solving the entire system in one step. Therefore, unlike the above use of operator splitting in decoupling two or more physical processes, we start with splitting the large-scale chemical kinetics in terms of the involved species. Once the participating

* Corresponding author.
E-mail addresses: jianhang.wang@tum.de (J.-H. Wang), shucheng.pan@tum.de (S. Pan), xiangyu.hu@tum.de (X.Y. Hu), nikolaus.adams@tum.de (N.A. Adams).

https://doi.org/10.1016/j.combustflame.2019.03.036

species of the large mechanism have been clustered into subsets of a smaller and equal size, an implicit solver can be applied to each group with significantly reduced matrix dimension. To minimize the splitting error, diffusion maps [22–24] are utilized to analyze the pairwise interaction relations of species by constructing a weight or similarity matrix of chemical kinetics, such that strongly interacting and mutually dependent species can be clustered into the same group. To partition the species into equal clusters, a balanced k-means algorithm [25] is employed.

The paper is organized as follows. In Section 2, we introduce the ODE system of chemical kinetics and formulate the species-clustered solver illustrated by a simple model example. Results from the proposed method for three detailed mechanisms in varying scales are presented and discussed in Section 3, considering the 0D auto-ignition problem at constant-volume and adiabatic conditions. Conclusions are drawn in Section 4.

2. Methodology

2.1. Operator splitting by species for chemical kinetics

The ODE system for chemical kinetics under adiabatic and constant-volume conditions can be expressed as

$$\frac{\mathrm{d}y_i}{\mathrm{d}t} = \frac{\dot{\omega}_i}{\rho}, \quad i = 1, \ldots, N_s, \tag{1}$$

where y_i and $\dot{w}_i$ denote the mass fraction and the total production rate of species i, respectively, in a mechanism consisting of N_s species and N_r reactions. Each reaction can be written as

$$\sum_{i=1}^{N_s} \nu_{ji}^f X_i \Longleftrightarrow \sum_{i=1}^{N_s} \nu_{ji}^b X_i, \quad j = 1, \ldots, N_r, \tag{2}$$

where ν_{ji}^f and ν_{ji}^b are the stoichiometric coefficients of species i appearing as a reactant and as a product in reaction j. The total production rate of species i in Eq. (1) is the sum of the production rate from each single elementary reaction

$$\dot{\omega}_i = W_i \sum_{j=1}^{N_r} (\nu_{ji}^b - \nu_{ji}^f) \left[k_j^f \prod_{l=1}^{N_s} \left[\frac{\rho_l}{W_l}\right]^{\nu_{jl}^f} - k_j^b \prod_{l=1}^{N_s} \left[\frac{\rho_l}{W_l}\right]^{\nu_{jl}^b} \right], \tag{3}$$

with k_j^f and k_j^b denoting the forward and backward reaction rates of each chemical reaction, and W_i being the molecular weight of the ith species and the partial density $\rho_l = y_l \rho$. With fixed total density and constant specific internal energy, the equation of state (EoS) for an ideal gas mixture can be used to determine the evolution of mixture temperature and thus to close the system.

The solution vector $\Phi = \{y_1, \ldots, y_{N_s}\}^T$ at time level n is integrated through the above ODE system for one timestep of Δt with the implicit solver VODE [9] to obtain

$$\Phi^{n+1} = R_{\Delta t}(\Phi^n). \tag{4}$$

The operator R represents the time integration by VODE. Upon operator splitting by species, we obtain

$$\Phi^{n+1} = R_{\Delta t}(\Phi_1^n) \circ R_{\Delta t}(\Phi_2^n) \cdots \circ R_{\Delta t}(\Phi_N^n), \tag{5}$$

corresponding to the Lie–Trotter splitting scheme [26], where Φ_k denotes the mass fractions of the species clustered in subset S_k out of N subsets in total. Clustering of species in each subset obeys

$$\begin{aligned} &\Phi = \{\Phi_1, \ldots, \Phi_N\}^T, \\ &S = \cup_{k=1}^N S_k, \ \ S_i \cap S_j = \emptyset \text{ if } i \neq j. \end{aligned} \tag{6}$$

Each subset of species cluster should have no overlap with others, and an almost equal number of species in each subset is assumed varying by at most one species, which requests a balanced partition/clustering algorithm [25]. The extension to higher-order splitting of Strang [27] is straightforward but inevitably more time consuming. Recalling that the scaling of computational cost to the number of species or the size of the kinetic mechanism involved using an implicit solver such as VODE is [4]

$$t_{\mathrm{CPU}} \sim \mathcal{O}\left(N_s^2\right) \text{ to } \mathcal{O}\left(N_s^3\right), \tag{7}$$

the total cost after species splitting can be reduced to

$$t_{\mathrm{CPU}}^{'} \sim \mathcal{O}\left(\frac{N_s^2}{N}\right) \text{ to } \mathcal{O}\left(\frac{N_s^3}{N^2}\right), \tag{8}$$

assuming equal computational consumption for each subsystem after species-splitting. A large mechanism consisting of ten thousand species, e.g., split the system into ten clusters with the Lie–Trotter scheme, results in a computational speedup of ten to a hundred times, without the need for additional sparse matrix techniques [12,13,28].

The essence of operator splitting by species for chemical kinetics lies in clustering species into subsets, each corresponding to a sub-ODE-system to be integrated by VODE or other implicit solvers. The merits of operator splitting by species are improved speedup of computational efficiency without changing the implicit solver, fast convergence and numerical stability [21].

2.2. Graph-based species clustering

A chemical reaction system with multiple species and reactions can be translated to a bi-partite graph [29], in which two sets of nodes represent the chemical species and reactions. Herein, we simply consider a finite graph consisting of the chemical species only and the non-linear coupling between pairs of species through reactions is abstracted as undirected edges linking every two nodes of species. For the sake of illustration, we consider $N_s = 6$ six species, {*A, B, C, D, E, F*}, and six first-order one-way reactions, i.e.

$$\begin{aligned} &A \xrightarrow{k_1} C, \ \ B \xrightarrow{k_2} C, \ \ C \xrightarrow{k_3} B, \\ &D \xrightarrow{k_4} C, \ \ E \xrightarrow{k_5} D, \ \ F \xrightarrow{k_6} D, \end{aligned} \tag{9}$$

where $k_1, \ldots, k_6$ are constant reaction rates. The exact solution for this problem can be easily obtained using symbolic computations of MATLAB® [30].

First we construct the graph of species, Fig. A.1(a). We may have two different clusterings I and II with two subsets ($N = 2$). Clustering I in Fig. A.1(b) is obtained by cutting off the link between species *C* and *D*. The strong couplings within clusters {*A, B, C*} and {*D, E, F*} are preserved. Upon clustering loosely coupled {*A, E, F*} together and leave the rest to compose the other cluster, we obtain Clustering II. The distance in the graph between (*A, E*) or (*A, F*) is remote as they are separated by two other species. The difference of the two clusterings also reflects in the rearranged Jacobian matrices by the order of splitting and clustering as shown in Fig. A.1(c) and (d). We can see that for Clustering I, when solving the cluster of {*A, B, C*} first, only the effect of species *D* is considered as constant since k_4 is not within the sub-Jacobian matrix. When solving the other cluster {*D, E, F*} subsequently, species *A, B* and *C* have no effect due to the corresponding zero entries. In total, the splitting error is attributed to only one element in the Jacobian, i.e. the k_4 block (red color) in Fig. A.1(c). For Clustering II, the solution of the first cluster {*A, E, F*} introduces no splitting error, whereas errors will occur when solving the cluster {*B, C, D*}, due to first-order approximation of $k_1 y_A$ for the production of species *C* and $k_5 y_E + k_6 y_F$ for the production of species *D*.

Numerical tests, in Fig. A.2, show that Clustering I agrees quite well with the exact solution, while Clustering II underestimates both the mass fractions of species *C* and *D*. This observation is in agreement with the previous discussion about operator splitting.

Given a prescribed number of clusters *N*, there are many possible clustering combinations. One simple strategy is to cluster the

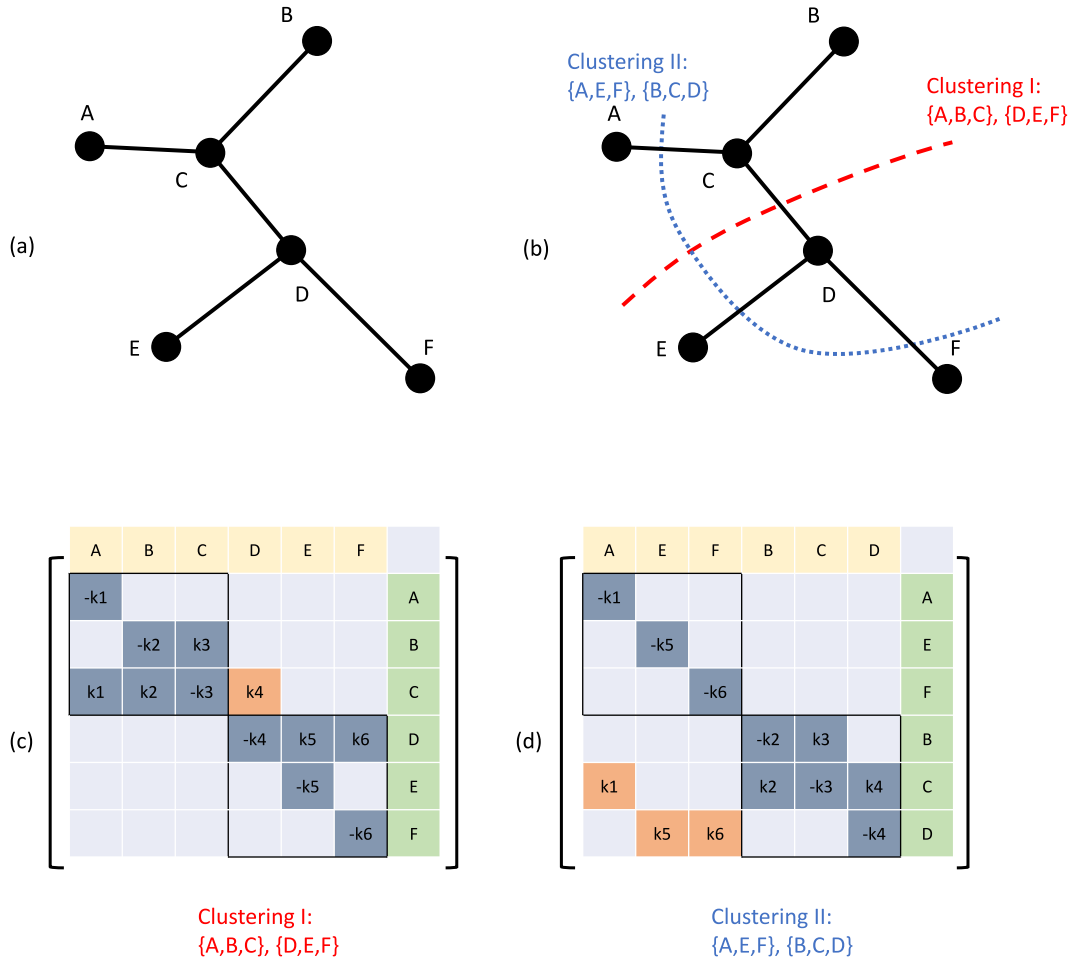

Fig. A.1. Reaction system example for species clustering. (a) Each node represents one species in {*A, B, C, D, E, F*}, and the edge, e.g., *e*(*A, C*), indicates that linked two species participate in at least one reaction as reactant or product; (b) two equal-sized clusterings are easily obtained as ({*A, B, C*}, {*D, E, F*}) and ({*A, E, F*}, {*B, C, D*}) by cutting off corresponding edges; (c) rearranged Jacobian matrix in the order of Clustering I; (d) rearranged Jacobian matrix in the order of Clustering II.

species according to species indices appearing in the mechanism. Another very promising strategy is to cluster all 'close' nodes in the graph into a subset, corresponding to having species with strong interactions in the same cluster. In this paper, we introduce diffusion maps [22–24] as a non-linear technique for dimensionality reduction, data set parameterization and clustering, to serve the purpose.

Let $G = (\Omega, W)$ be a finite graph of n nodes, where the weight matrix $W = \{w(x, y)\}_{x,y\in\Omega}$ is symmetric and component-wise positive [23]. The definition of weight matrix needs to reflect the degree of affinity of nodes x and y. Diffusion maps start with a user-defined weight matrix and utilize the idea of Markov random walk to describe the connectivity of nodes through a diffusion process. For technical details of diffusion maps, we refer to [22–24].

For the above reaction system, we define, with the help of species graph in Fig. A.1(a), the weight matrix W by

$$w(x,y) = \begin{cases} max(k_j), & \text{if } x \text{ and } y \text{ both participate in reaction } j, \\ \epsilon, & \text{otherwise,} \end{cases} \tag{10}$$

where ϵ takes a small positive value to avoid zero entries, e.g., $\epsilon = 10^{-12}$. The diagonal elements in the weight matrix, $w(x, x)$, can be defined as

$$w(x,x) = max(w(x,y)_{y\neq x}). \tag{11}$$

In combination with the reaction rates given in Fig. A.2, the weight matrix obtained by the above definition is shown in Fig. A.3. Using diffusion maps to analyze the graph based on our defined weight matrix, we can project the set of species into a diffusion space with at most n dimensions, where the pairwise distance reveals the connectivity between two species. In Fig. A.3, it is shown that the species are projected onto a x_1x_2 plane using the first two dimensions of the diffusion space. We can see that species *A, B* and *C* almost collapse into one point and locations of species *D, E* and *F* in the x_1 direction (which is also the first and dominant dimension) are also very close to each other. Their coordinates in the second dimension separate the three species. However, the centroids of subset {*A, B, C*} and subset {*D, E, F*} are far from each other. Accordingly, a straightforward clustering using the k-means algorithm (setting $k \equiv N = 2$) can be easily obtained, i.e. ({*A, B, C*}, {*D, E, F*}). This clustering from diffusion maps is the same as the previous Clustering I, indicating that it is the optimal case of two clusters for the reaction system above with minimum splitting errors. In Fig. A.2, we can also observe that exact mass conservation is violated by operator splitting with first-order convergence rate using the Lie–Trotter scheme. However, the optimal Clustering I has a significantly lower mass conservation error than Clustering II. An additional treatment for the correction of mass-conservation errors as in [11] can be applied. In this illustrative example, it should be noted that the underlying fact of $k_4 = 1$ being quite small benefits Clustering I through the weight matrix W in Eq. (10). If k_4 becomes larger, both the previous manual clustering and the current diffusion maps based clustering would be different, with the coupling between species *C*

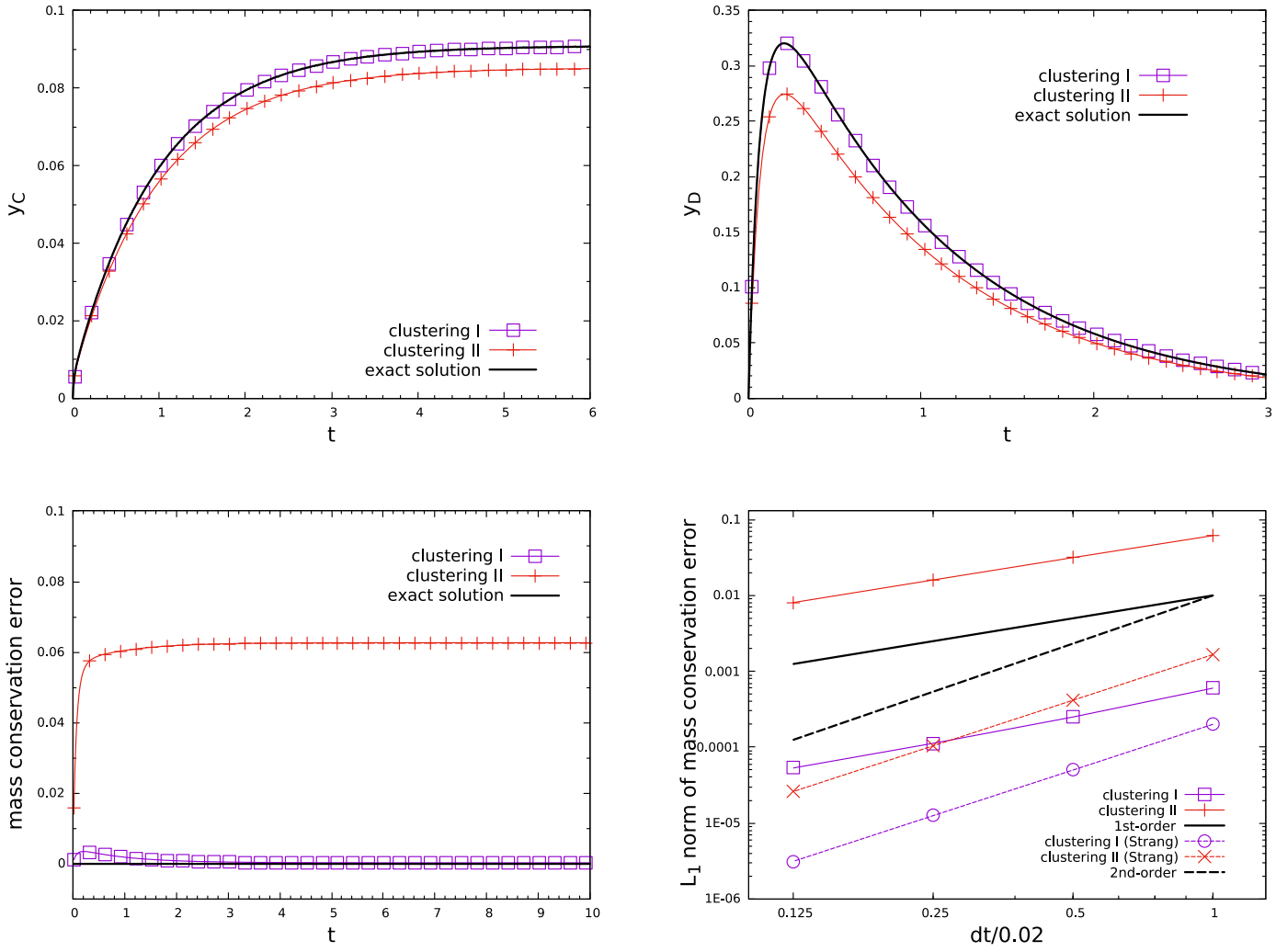

Fig. A.2. Numerical integration results with two clusterings by Lie–Trotter and Strang splittings, compared with the exact solution. Reaction rates are $k_1 = 1, k_2 = 10, k_3 = 100, k_4 = 1, k_5 = 10, k_6 = 20$, and the initial condition is $y_A = 0.6, y_E = 0.2, y_F = 0.2$ with zero mass fractions of *B, C, D*. The base timestep size is $\Delta t = 0.02$.

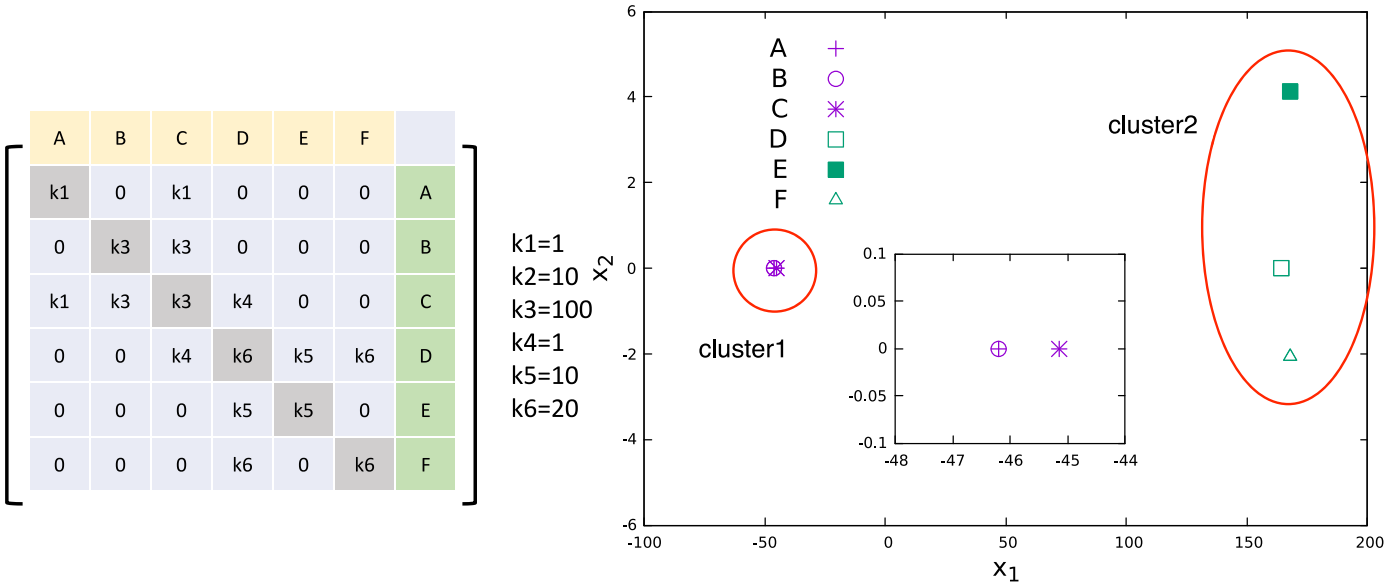

A	B	C	D	E	F	
k1	0	k1	0	0	0	A
0	k3	k3	0	0	0	B
k1	k3	k3	k4	0	0	C
0	0	k4	k6	k5	k6	D
0	0	0	k5	k5	0	E
0	0	0	k6	0	k6	F

k1=1
k2=10
k3=100
k4=1
k5=10
k6=20

Fig. A.3. Weight matrix of diffusion maps for the reaction system (left); embedding and clustering of species in 2D diffusion space (right).

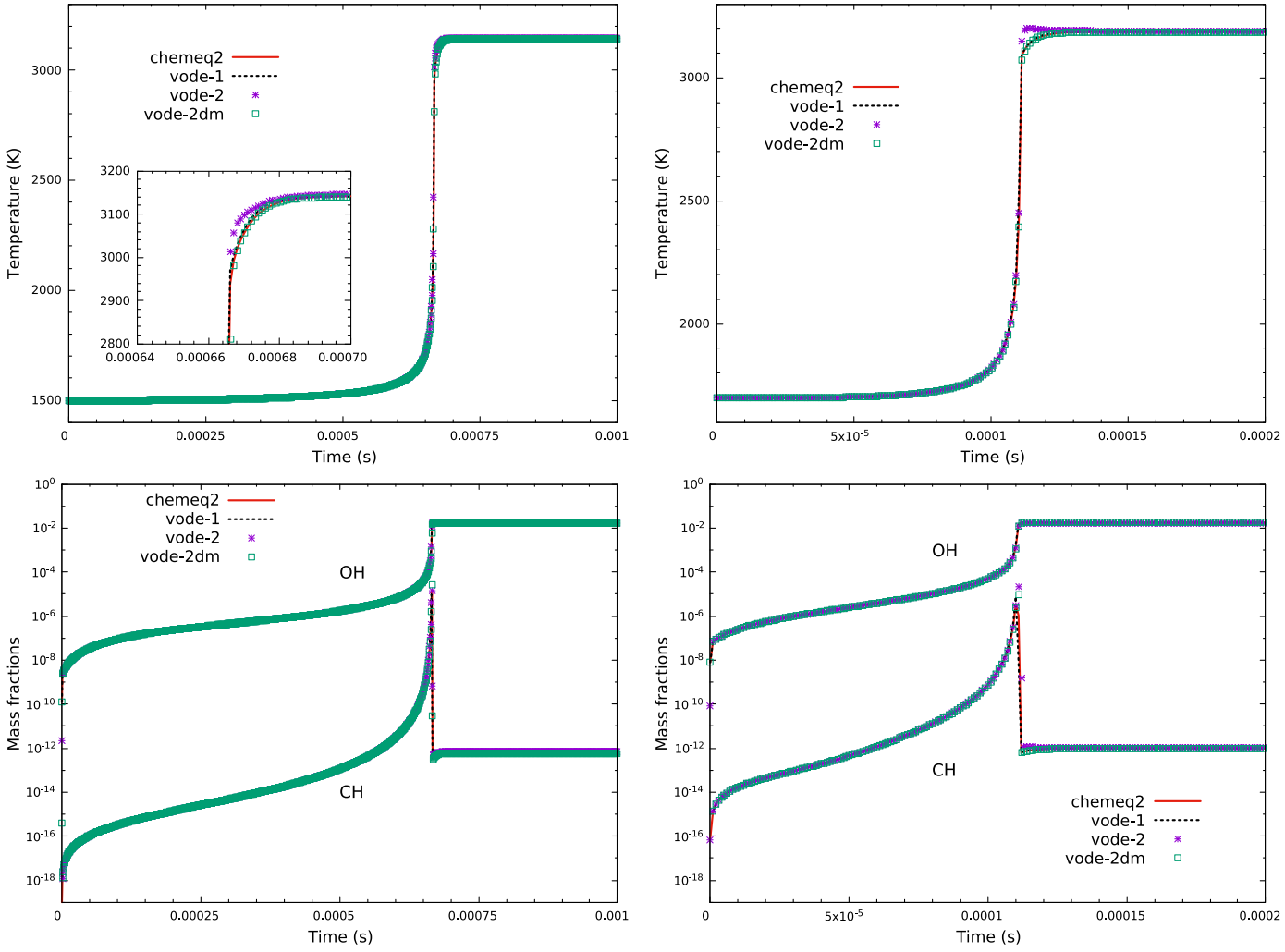

Fig. A.4. Calculated temperature and mass fraction histories for methane/air ignition delay problem in two initial conditions: left column (Case 1) and right column (Case 2).

and D to be preserved and both being clustered into the same subset.

For much more complicated realistic chemical kinetics especially involving fuel combustion mechanisms, reaction rates are not always constant but depend on temperature or even pressure of the mixture. This normally can be expressed by the finite-rate Arrhenius model [31,32] and thus the weight matrix as above should also take into account the varying reaction rates with temperature. Rather than sampling at a single temperature, e.g., the initial temperature of an auto-ignition problem of combustible gas mixtures, we take many temperature samples in order to construct a representative weight matrix. The derived clustering by diffusion maps based on such a weight matrix can be stored and used for other conditions as long as the same mechanism is involved. In such way, the determination of the weight matrix as well as the clustering procedure can be treated as a preprocessing step instead of costly on-the-fly clustering. Since multiple scales of the absolute reaction rates exist, usually spanning several orders of magnitude, logarithmic scaling of the reaction rates can be performed to avoid underestimating the slow reactions. Also, normalization in each row of the matrix relative to the diagonal species is carried out as

$$w(x,y) = \frac{w(x,y)}{w(x,x)}, \tag{12}$$

Table 1
Numbers of species and reactions in detailed mechanisms.

	No. of species	No. of reactions
CH_4	53	325
n-C_7H_{16}	561	2539
n-$C_{16}H_{34}$	2115	8157

and

$$w(x,y) = max(w(x,y), w(y,x)) \tag{13}$$

for all species pairs is further checked to guarantee the symmetry of weight matrix in the diffusion maps.

3. Numerical results and discussion

In this section with numerical experiments, we consider three detailed mechanisms for hydrocarbon fuel combustion: the GRI-Mech 3.0 mechanism for methane (CH_4) [33], the n-heptane (n-C_7H_{16}) mechanism (Version 2) [34,35], and the n-hexadecane (n-$C_{16}H_{34}$) mechanism [36]. The dimensions of three mechanisms are listed in Table 1, exhibiting increasing numbers of species and reactions as well as growing computational complexity of time integration. Zero-dimensional auto-ignition of the fuel/air mixture under adiabatic and constant-volume conditions is taken into consideration.

Table 2
Initial conditions for methane/air mixture.

	CH_4–O_2–Ar molar ratio	Temperature (K)	Pressure (atm)
Case 1	9.1–18.2–72.7%	1500	1.8
Case 2		1700	2.04

3.1. Methane/air auto-igniton

The first example considers the ignition delay problem of methane/air mixture. Two different initial conditions [37] are considered as in Table 2. For Case 1, the computation is carried out until $t = 0.001$ s and the timestep size is fixed at $\Delta t = 1 \times 10^{-7}$ s (this timestep size is also adopted for other cases and is comparably large for compressible and reactive CFD analysis). The computation of Case 2 is until $t = 2 \times 10^{-4}$ s. CHEMEQ2 [31] as a popular explicit ODE solver for chemical kinetics is also employed here for reference, together with the implicit solver VODE. In CHEMEQ2, the convergence parameter of the predictor–corrector method is 1×10^{-4}. In VODE, the relative and absolute error thresholds (RTOL and ATOL) are 1×10^{-5} and 1×10^{-13}, respectively. Since the dimension of the methane mechanism is relatively small, we cluster the 53 species into two subsets, and each cluster of species is integrated by VODE by operator splitting as in Eq. (5). Accuracy and convergence of the splitting method using species clustering are examined by this example. Benefits of computational efficiency from operator splitting by species clustering is to be tested by the following two mechanisms of much larger dimensions. As an important parameter to measure the accuracy of mechanism and ODE solver, ignition delay times, t_{ign}, for the two cases can be referred to [37], i.e. $t_{ign} = 666$ ms for Case 1 and $t_{ign} = 110$ ms for Case 2.

To validate operator splitting by species, the results obtained by CHEMEQ2 and VODE with/without species clustering are shown in Fig. A.4, where VODE-1 is without species clustering (that is, all the species are solved in a single set and a single step) while both VODE-2 and VODE-2dm partition the species into two clusters for operator splitting by setting $N = 2$. The difference of clustering is that VODE-2 simply clusters the species in accordance with the species' index in the mechanism (e.g., species of odd or even indexing numbers are clustered in different subsets) while VODE-2dm utilizes diffusion maps for species clustering based on the weight matrix defined in Eqs. (10)–(13), see Appendix A. In general, clustering based on the indices of species can be readily obtained by

$$\text{Species } i \in \begin{cases} \text{cluster } 1: & \text{if } mod(i,N) = 1, \\ \text{cluster } 2: & \text{if } mod(i,N) = 2, \\ \cdots & \\ \text{cluster } N-1: & \text{if } mod(i,N) = N-1, \\ \text{cluster } N: & \text{if } mod(i,N) = 0, \end{cases} \tag{14}$$

where i denotes the ith species in the mechanism and N is the number of clusters by partition. It can be seen that all four solutions give the correct ignition delay times in two cases. For Case 1, VODE-2 overestimates the temperature slightly before it reaches an equilibrium state while VODE-2dm has nearly the same temperature with both CHEMEQ2 and VODE-1. The deficiency of VODE-2 solution is larger in Case 2, which also occurs at the end of the ignition process. Different predictions by VODE-2 and VODE-2dm can be attributed to the splitting error: with diffusion maps, the error in VODE-2dm is smaller than that in VODE-2. This can be illustrated by embedding the clustered species into a diffusion space, as shown in Fig. A.5. As the clustered species are projected into the 3D diffusion space, we can clearly see that the two clusters of species are separated from each other using diffusion maps, which indicates that each cluster is able to preserve the close interactions between coupling species. In particular, for the VODE-2dm clustering, the first species H and the last species CH_3CHO are within the same cluster as the 13th species CH_3, due to the high activity of H which is involved in composition or decomposition reactions with hydrocarbon species such as

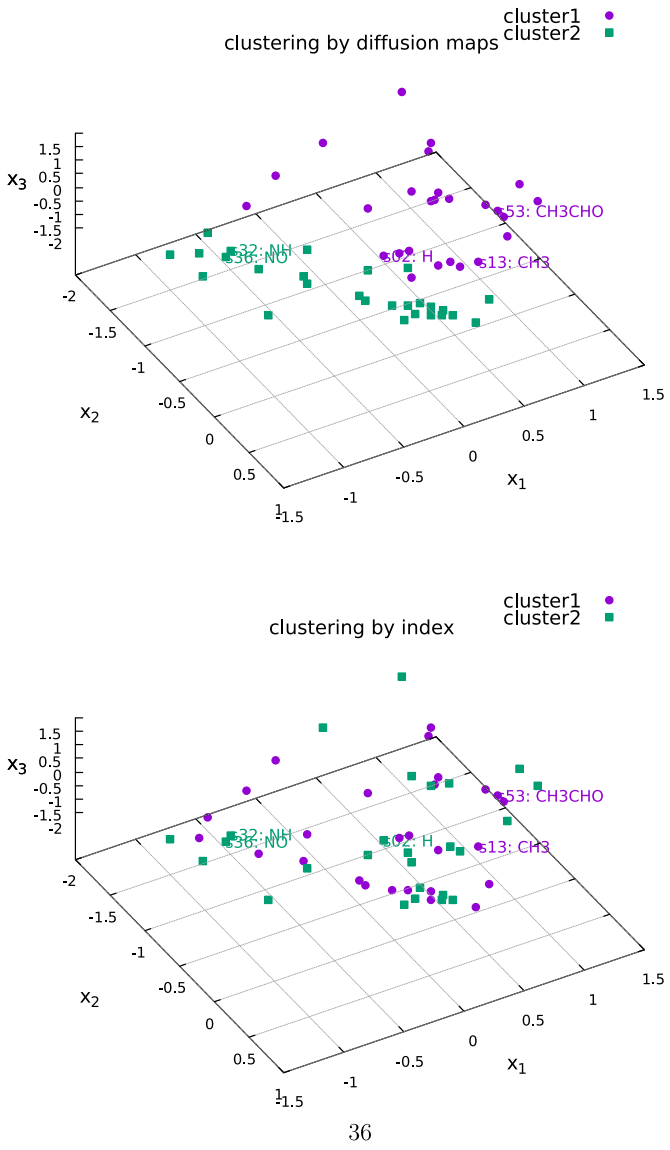

Fig. A.5. Embedding with first three diffusion coordinates of species for methane mechanism.

$$O + C_2H_5 \Longleftrightarrow H + CH_3CHO,$$
$$H + CH_3(+M) \Longleftrightarrow CH_4(+M).$$

Also, playing a critical role in the mechanism (as it participates in a large number of reactions), H is located at the center of the diffusion map among all the species. On the other hand, species such as NO and NH are clustered into the other subset because they mainly participate in nitrogen-related reactions, with weaker interactions with hydrocarbon species. In contrast, H is clustered into the NH and NO group in the VODE-2 clustering by index. The obtained two clusters merge each other in the diffusion map, and some pairs of two species with short distances are divided into different clusters, leading to larger splitting error with VODE-2 than with VODE-2dm.

We examine convergence of the splitting method by varying the fixed timestep adopted in Fig. A.6. It can be seen that as the timestep decreases the evolution of temperature and mass fractions approach the corresponding profiles at the shortest timestep:

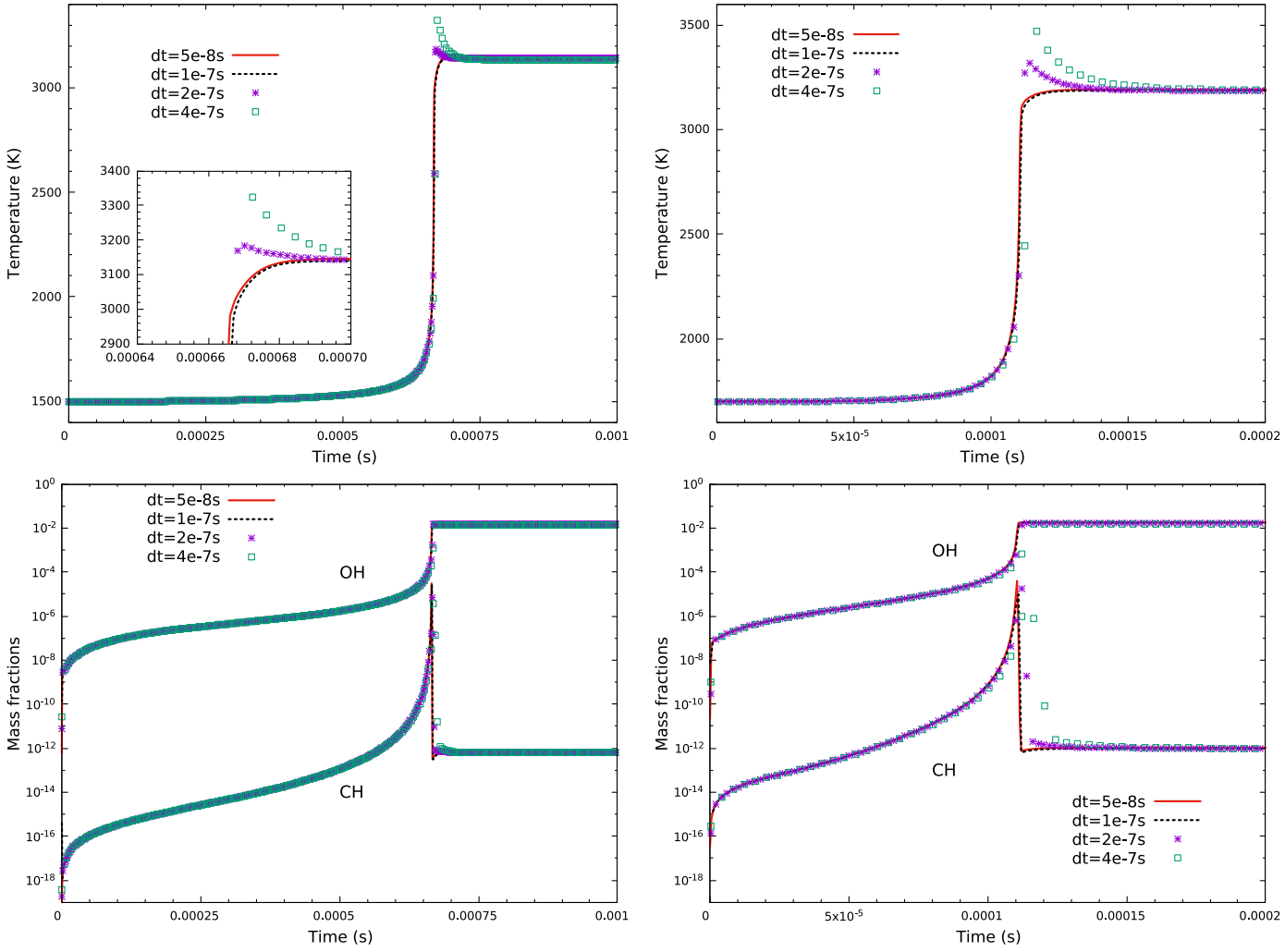

Fig. A.6. Calculated temperature and mass fraction histories for methane/air ignition delay problem by species clustering using varying timesteps in two initial conditions: left column (Case 1) and right column (Case 2).

Table 3
Initial conditions for n-heptane/air mixture.

	n-C_7H_{16}:O_2:N_2 (mole)	Temperature (K)	Pressure (atm)
Case 3	0.09091:1:3.76	1250	10
Case 4			50

spikes in the temperature profiles with large timesteps gradually disappear and the jumps of mass fraction, y_{CH}, tend to sharpen due to sudden consumption during the ignition process. The timestep size of $\Delta t = 1 \times 10^{-7}$ s is verified to be sufficient for integrating the chemical kinetics correctly.

3.2. n-Heptane/air auto-igniton case

The second example considers the n-heptane/air combustion mechanism. Two different initial conditions [38] are considered as in Table 3. For Case 3, the computation is carried out until $t = 4 \times 10^{-4}$ s and the timestep size is fixed at $\Delta t = 1 \times 10^{-7}$ s. The computation for Case 4 is until $t = 1.1 \times 10^{-4}$ s. Without a prior knowledge of the number of clusters which is most suitable and efficient for computing this large-scale mechanism, we choose to split the species by eight clusters using diffusion maps first.

In Fig. A.7, the species clustered VODE result using diffusion maps is compared with that of simple clustering using Eq. (14) by setting $N = 2, 4$ and 8, respectively, and also the results by CHEMEQ2 and non-split VODE. Calculated ignition delay times observed from the temperature histories of Case 3 and 4 by CHEMEQ2, VODE-1 as well as VODE-8dm agree well with each other and also with the numerical results in Ref. [38]. Using the simple clustering algorithm instead of diffusion maps, VODE-2, VODE-4 and VODE-8 obtain the correct ignition delay time for Case 3 while they all severely over-predict the delay of ignition for Case 4. Although the ignition delay time is not very sensitive to the species clustering in Case 3, the post-ignition equilibrium state appears to depend strongly on the quality of the clustering, as we can see that both VODE-2 and VODE-4 overestimate the equilibrium temperature incorrectly and VODE-8 induces an incorrect spike before the temperature reaches the equilibrium state, which is similar with the example of methane combustion. For Case 4, extremely high equilibrium temperatures nearly 4000 K and higher are predicted by VODE-2 and VODE-4, and temperature spike also can be seen for the VODE-8 solution. To explain the over/under-estimation of the equilibrium temperature as well as the delayed ignition times resulted from simple clusterings, we refer to the time-dependent total mass conservation errors in Fig. A.8. As previously stated in Fig. A.2 for the illustrative example, species-clustered splitting might violate total mass conservation because it will inevitably cut off some pathways/channels within coupled species. It is observed that mass conservation

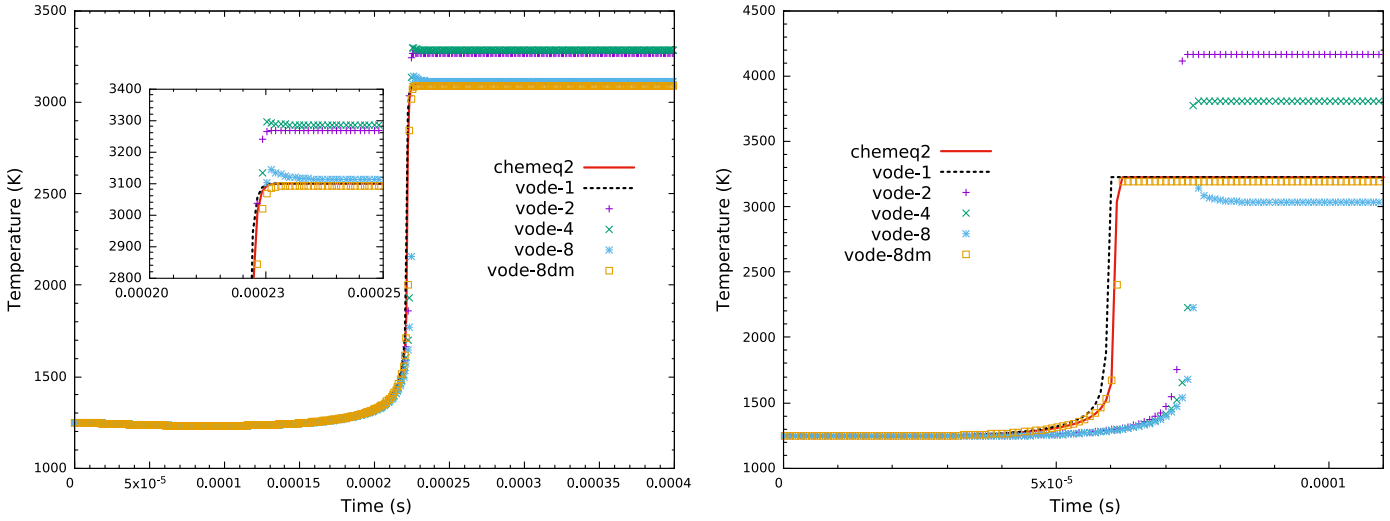

Fig. A.7. Calculated temperature histories for n-heptane/air ignition delay problem in two initial conditions: left column (Case 3) and right column (Case 4).

Table 4
CPU times (s) for clusters at different clustering number N for Case 4.

N	Total									Max.	Min.	Ave.
1	283.407527									283.407527	283.407527	283.407527
2	77.981967	24.689422	53.052336							53.052336	24.689422	38.870879
4	43.336673	11.065684	18.228123	6.475912	7.314687					18.228123	6.475912	10.7711015
8	62.65253	6.059054	5.854662	9.995675	5.960626	5.253225	7.319861	7.693178	14.218079	14.218079	5.253225	7.794295

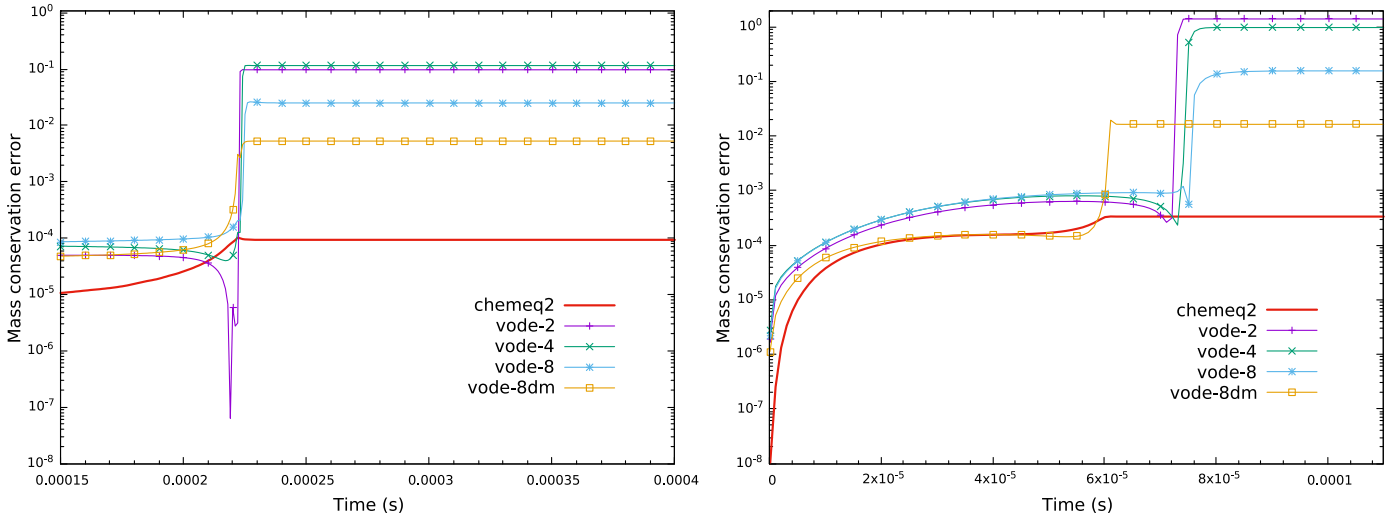

Fig. A.8. Total mass conservation error ($|\sum y_i - 1|$) histories for n-heptane/air ignition delay problem in two initial conditions: left column (Case 3) and right column (Case 4).

errors are very small before ignition, and as ignition triggers them to increase, mass conservation errors reach a relatively high plateau after ignition. We also observe that VODE-8dm yields obviously less conservation errors compared with other simple clusterings, corresponding to less splitting errors. In comparison, CHEMEQ2 produces orders of magnitude smaller errors than the present VODE-8dm and VODE-1 preserves the mass conservation up to roundoff errors (not shown in the figure). Therefore, although the proposed VODE-8dm outperforms other simple clusterings by largely reducing the splitting errors, there is room for further improvement.

In Fig. A.9, we present the species embedding with the first three coordinates, leading to eight clusters of species being scattered but compact in the diffusion space. In comparison, the simple clustering by indices produces disorder species in the diffusion space. The quality of such a simple clustering is therefore expected to be poor, as shown in Fig. A.7. Since the weight matrix is kept unchanged for the same mechanism, the diffusion space containing all the species is also the same and independent of the number of clusters one wants to partition. It is straightforward to further combine the close subsets (every two or four) into a larger cluster so that clustering by $N = 4$ and $N = 2$ can be obtained.

Next, we compare the results denoted by VODE-2dm and VODE-4dm in Fig. A.10. It can be seen that for both cases, the diffusion-map based results all capture the correct ignition delay time and the equilibrium temperature. In particular, the VODE-2dm result performs better than the CHEMEQ2 result, being closer to the non-split VODE-1 result. As the number of partition/splitting decreases, the split VODE results consistently approach the non-split solution, with reduced splitting errors.

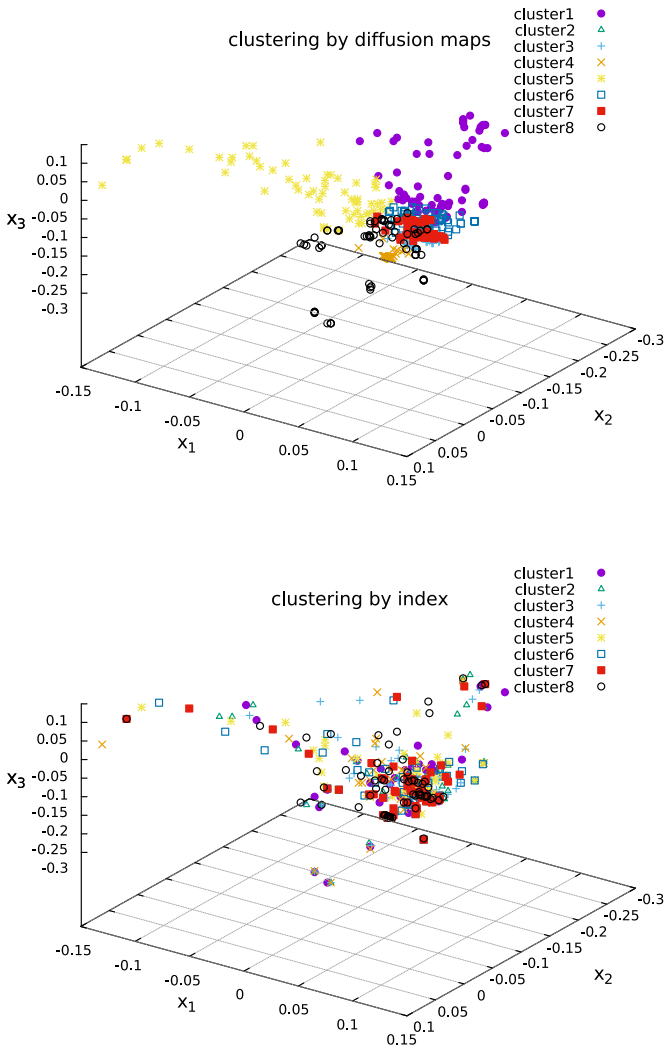

39

Fig. A.9. Species distribution in the diffusion space with first three diffusion coordinates of species for n-heptane mechanism.

In Fig. A.11 (left), we investigate the computational efficiency of different solvers. All the results are normalized based on the CPU time of VODE-1. It is to be noted that in these two cases, the non-split VODE solver is faster than CHEMEQ2. For the split VODE solver using diffusion maps, we can see the reduced CPU times with the increasing number of clusters up to $N = 4$ falls within the region bounded by two theoretical scalings according to Eq. (8). When the number of clusters increases to $N = 8$, the CPU time meets a turning point and the computational efficiency no longer monotonically decreases. Regarding the decay in computational efficiency, two facts should be noted:

- For the decoupled subsystems at a specific number of clusters N, although they share the equal number of species as in Eq. (6), species and their reactions/interactions within each subset are quite different such that Jacobian evaluation and LU factorization as well as the Newton iteration in the VODE solver for each subsystem consume different CPU times. As shown in Fig. A.11 (right) and Table 4, CPU times for subsystems at a given partition number exhibit very large diversity, leading to an imbalance of computational costs among clusters after species-splitting. The non-balanced computational costs contradict the 'ideal' balanced theoretical scaling in Eq. (8);
- When the number of clusters N is large and the dimension of each subsystem is small, CPU time of dense LU factorization ($\propto N_s^3$) no longer dominates the total CPU time. Instead, CPU times of Jacobian evaluation and Newton iteration (both $\propto N_s$) begin to exceed that of dense LU factorization; see in [12,19]. The 'ideal' theoretical scaling in Eq. (8) is no longer valid for large clustering numbers. Therefore, the averaged computational cost of a cluster in Fig. A.11 (right) exhibits high-order decrease rates ($\propto 1/N^2$ to $1/N^3$) for small N and then it linearly decreases with the decreasing number of species within each subsystem $\frac{N_s}{N}$ or the inverse of the clustering number N for larger N.

From Fig. A.11, $N = 4$ may be an optimal clustering number which weighs efficiency and accuracy for the n-heptane ignition problem. With VODE-4dm, we further investigate the ignition delay times of n-heptane oxidation based on a series of varying initial temperatures at 10 and 50 atm, respectively, in Fig. A.12. The negative temperature coefficient (NTC) behavior has been accurately reproduced, in excellent agreement with the results in Fig. 2 of [38].

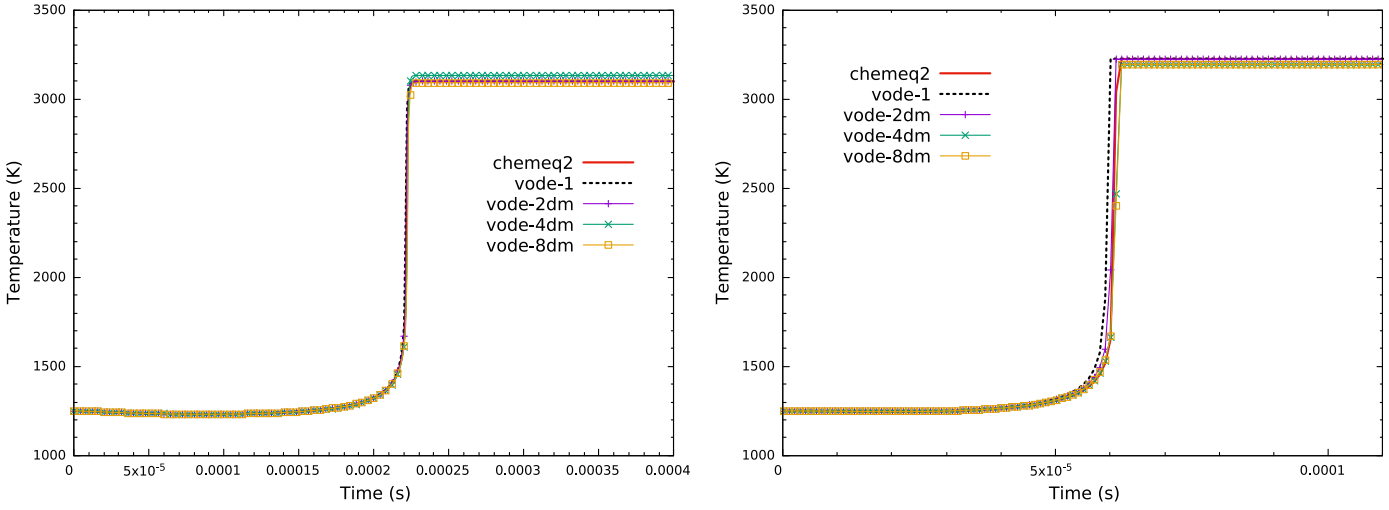

Fig. A.10. Calculated temperature histories for n-heptane/air ignition delay problem by species clustering setting $N = 2, 4, 8$ in two initial conditions: left column (Case 3) and right column (Case 4).

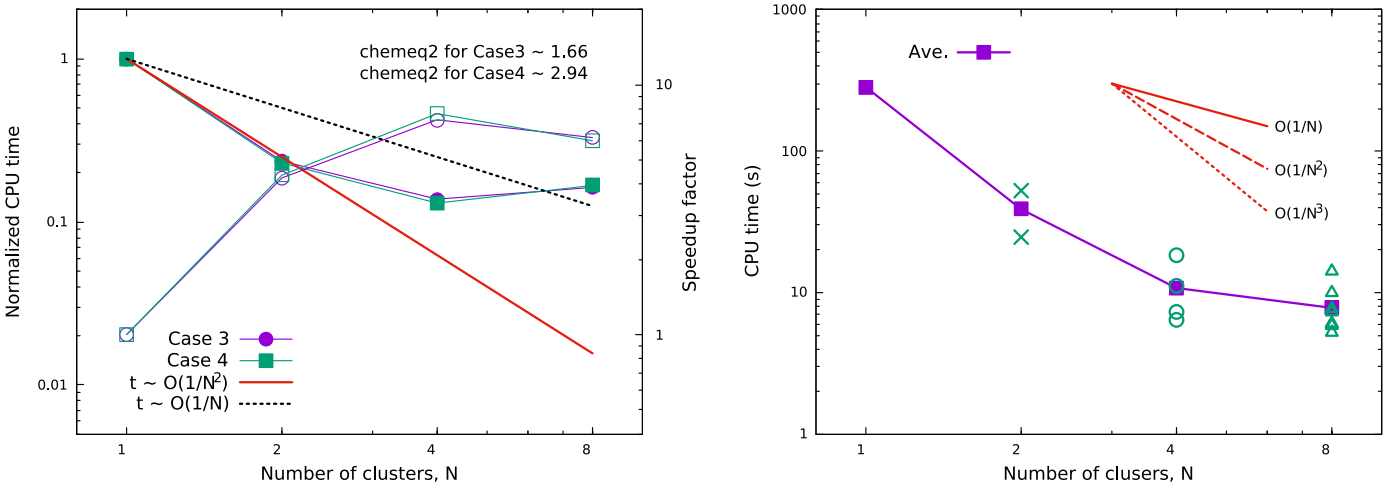

Fig. A.11. Left: normalized CPU time and speedup factor by species clustered VODE with $N = 1, 2, 4, 8$; CPU time is normalized by t/t_{vode1} and speedup factors use hollow symbols. Right: CPU time of each cluster by species clustered VODE with $N = 1, 2, 4, 8$ for Case 4.

Table 5
Initial conditions for n-hexadecane/air mixture.

	$n\text{-}C_{16}H_{34}:O_2:N_2$ (mole)	Temperature (K)	Pressure (bar)
Case 5	0.04082:1:3.76	1111.11	13.5
Case 6		1250	

3.3. n-Hexadecane/air auto-igniton case

The third example considers the n-hexadecane/air combustion mechanism with the largest dimension. Two initial conditions [39] are considered as in Table 5. For Case 5, the computation is carried out until $t = 1.1 \times 10^{-3}$ s while it is interrupted for Case 4 at $t = 2.2 \times 10^{-4}$ s with 2200 equal timesteps. We also choose to split the species by eight clusters using diffusion maps.

In Fig. A.13, the species clustered VODE result using diffusion maps is compared with that of simple clustering using Eq. (14) by setting $N = 2, 4$ and 8, respectively, and also with the results by CHEMEQ2 and non-split VODE. Calculated ignition delay times observed from the temperature histories of Case 5 and 6 by CHEMEQ2, VODE-1 as well as VODE-8dm agree well with each other and also numerical results of Ref. [39]. Using simple clustering algorithm instead of diffusion maps, VODE-2, VODE-4 and VODE-8 obtain three increasing ignition delay times for Case 3 and 4. VODE-8 computes the most delayed ignition time, and both

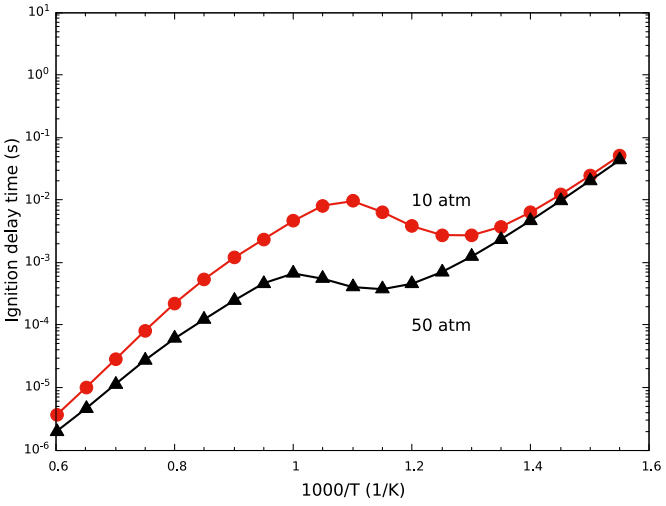

Fig. A.12. Ignition delay times based on different initial temperatures for the stoichiometric n-heptane/air mixture predicted by VODE-4dm.

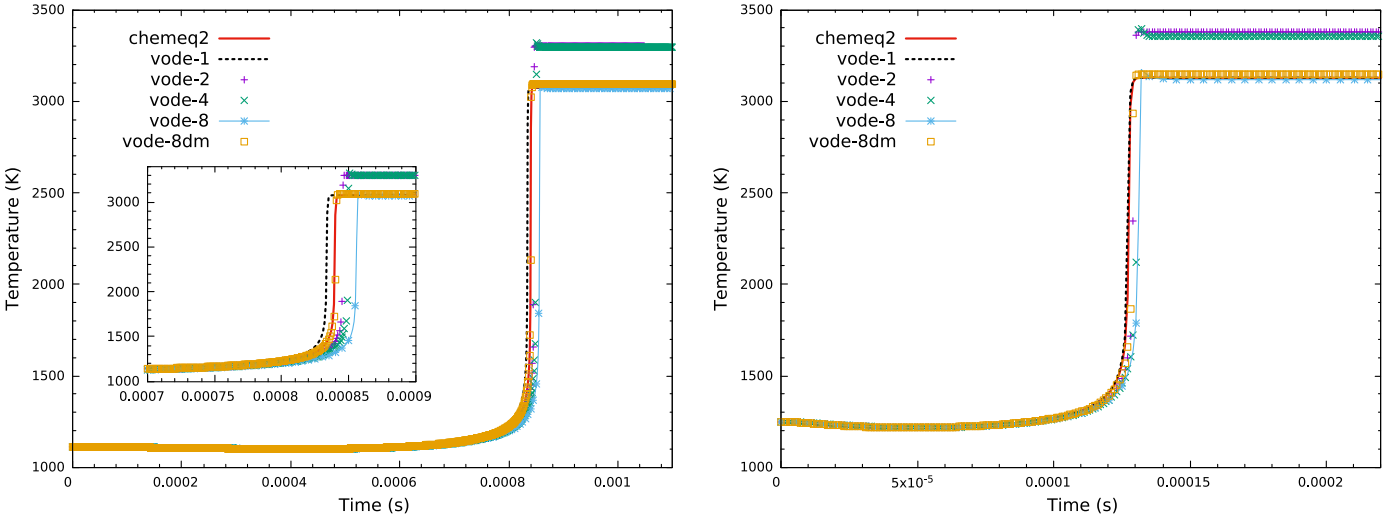

Fig. A.13. Calculated temperature histories for n-hexadecane/air ignition delay problem in two initial conditions: left column (Case 5) and right column (Case 6).

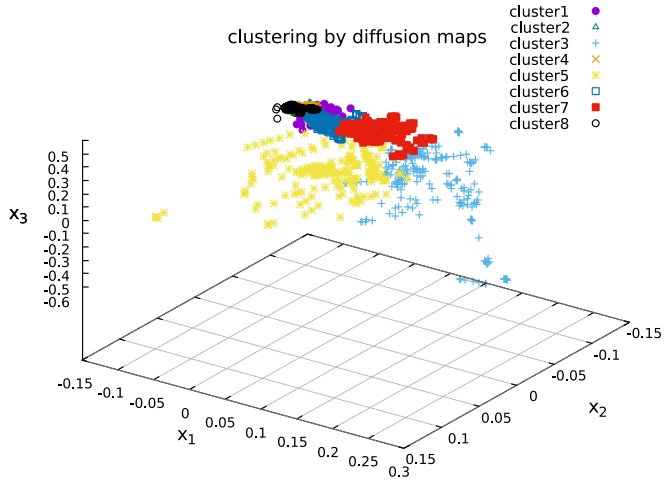

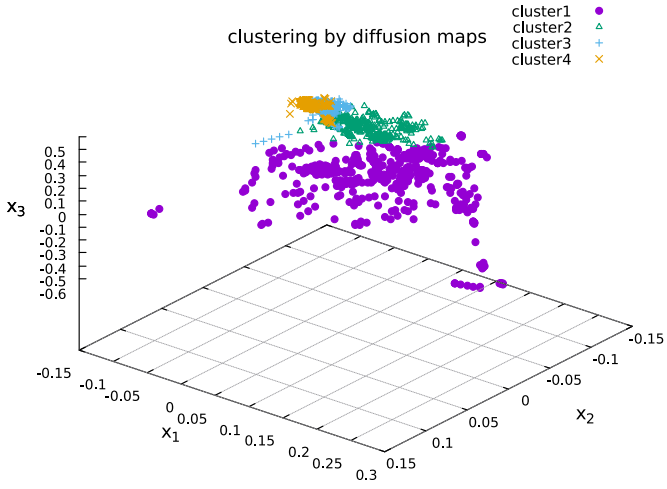

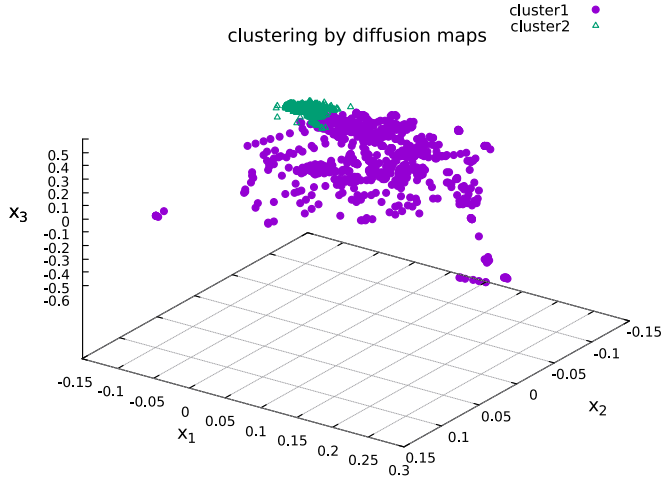

Fig. A.14. Species distribution in the diffusion space with first three diffusion coordinates of species for n-hexadecane mechanism.

VODE-2 and VODE-4 overestimate the equilibrium temperature after ignition incorrectly. In contrast, the VODE-8dm result is comparable with the CHEMEQ2 result in both the ignition and post-ignition process.

In Fig. A.14, we present the species embedding with the first three coordinates, leading to eight/four/two clusters of species being scattered in the diffusion space. It can be seen that the clustering with less number of clusters basically combines the close subsets of species into a larger cluster, as it is manually realized in the n-heptane example. By comparing the five results with different number of clusters up to $N = 16$ based on diffusion maps in Fig. A.15, it is demonstrated that for both cases, the diffusion maps based results all capture the relatively correct ignition delay time and the equilibrium temperature. In particular, the VODE-2dm result performs the best, even better than the CHEMEQ2 result, being closest to the non-split VODE-1 result. The VODE-16dm result slightly overestimates the equilibrium temperature and the ignition time predicted by VODE-8dm is later than that of VODE-4dm by 1×10^{-5} s roughly. Though, as the number of partition/splitting decreases, the split VODE results consistently approach the non-split solution, with reduced splitting errors.

In Fig. A.16 (left), we investigate again the computational efficiency of different solvers. CHEMEQ2 is more efficient than VODE in the first case while in the second case the non-split VODE solver is faster than CHEMEQ2, both solvers with the same order of magnitude of CPU time. Focused on the split VODE solver using diffusion maps, we can see the reduced CPU times as the number of clusters increases up to $N = 8$. The performance in terms of computation efficiency for the clustered VODE solvers when $N = 2$ or 4 even exceeds the theoretical expectation. It can be also explained by the large deviation of computational costs for single subsystems when $N = 2$ or 4. As shown in Fig. A.16 (right) and Table 6, at a given clustering number, the maximum CPU time for a cluster is larger than the minimum CPU time by nearly one order of magnitude in this n-hexadecane case. As a result, the total CPU time mainly depends on the maximum CPU time for a cluster: for the $N = 2$ clustering, its maximum CPU time for one cluster is approximately proportional to $\frac{1}{N^3}$, and it is between $\frac{1}{N^2}$ and $\frac{1}{N^3}$ if the maximum CPU time for one cluster in VODE-4dm is scaled in comparison to that of the non-split VODE-1. When $N = 8$ or 16, the deviation of CPU times for different clusters of equal size becomes smaller and thus its total CPU time, as a sum of CPU times for 8 or 16 clusters, falls into the theoretical zone, which also implies that $N = 8$ or 16 is a reasonable clustering number for the n-hexadecane mechanism.

When the number of clusters increases to $N = 16$, the CPU time no longer decreases, indicating $N = 8$ may be an optimal clustering number from the aspect of efficiency for the n-hexadecane ignition problem. A total speedup factor of around 40 is realized by VODE-8dm for Cases 5 and 6. It is about 50 times faster than CHEMEQ2 for the computation of Case 6.

4. Conclusions

For large-scale chemical kinetics involving many species and reactions, computational efforts needed for time integration usually exceeds linear scaling with the dimension of the kinetic mechanism, especially when implicit ODE solvers are used. To achieve a higher computational efficiency, we have proposed operator splitting to integrate the large system in separate yet consecutive subsystems of the same and smaller dimension. Each subsystem includes a cluster of species decoupled from the other species of the full mechanism and is solved separately, e.g., implicitly by VODE. In order to reduce the inevitable splitting error, diffusion maps are applied to analyze the species graph and to cluster strongly coupled species into the same subsystem, by defining an appropriate

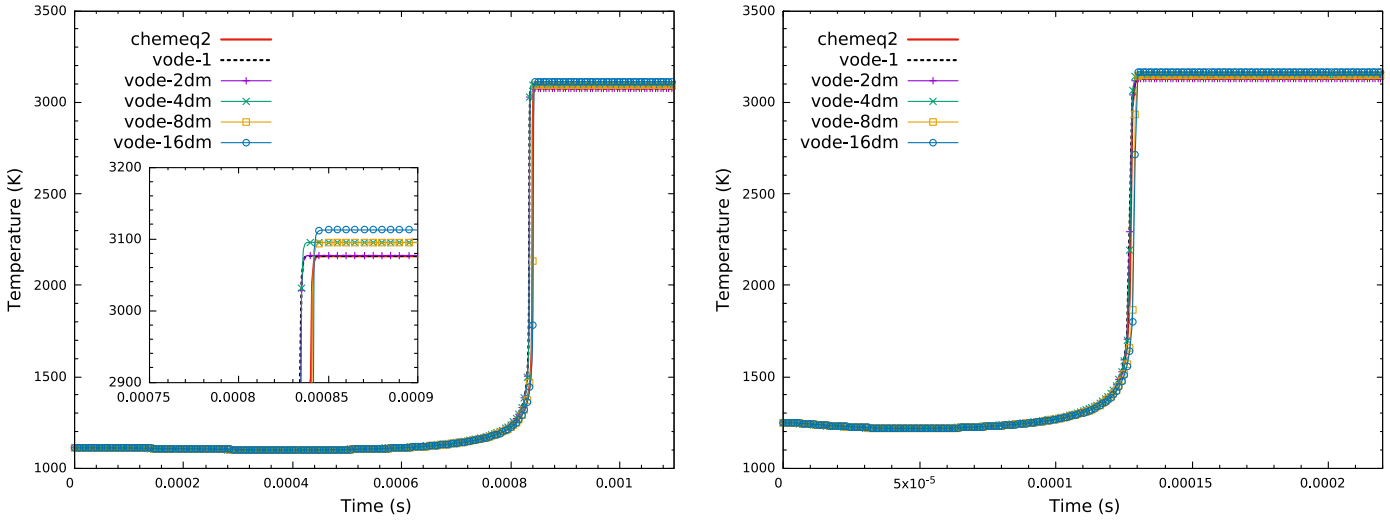

Fig. A.15. Calculated temperature histories for n-hexadecane/air ignition delay problem by species clustering setting $N = 2, 4, 8, 16$ in two initial conditions: left column (Case 5) and right column (Case 6).

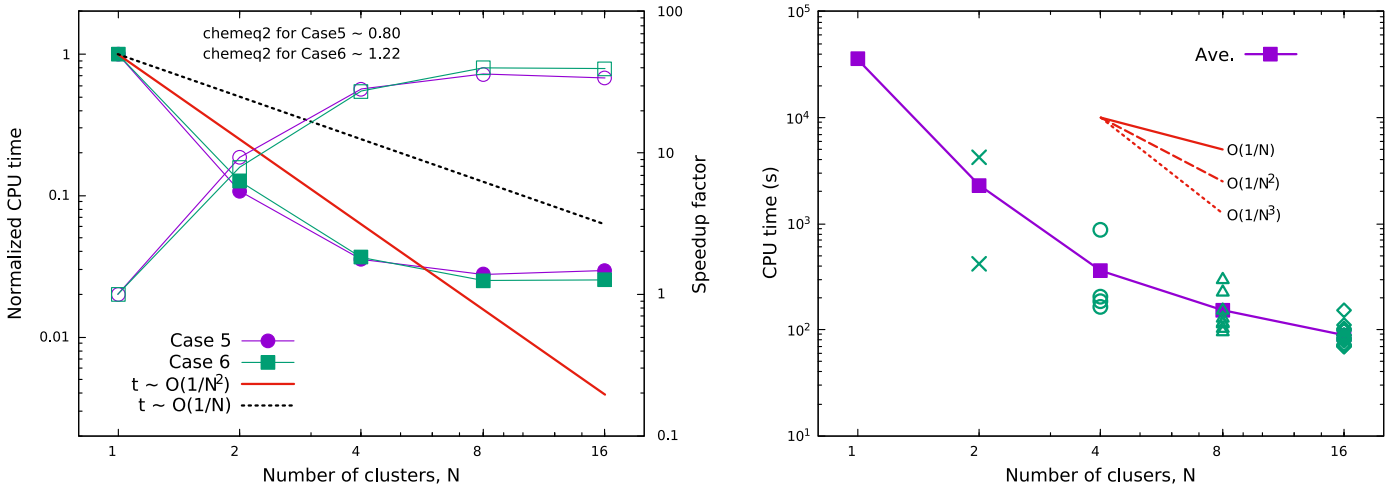

Fig. A.16. Left: normalized CPU time and speedup factor by species clustered VODE with $N = 1, 2, 4, 8, 16$; CPU time is normalized by t/t_{vode1} and speedup factors use hollow symbols. Right: CPU time of each cluster by species clustered VODE with $N = 1, 2, 4, 8, 16$ for Case 6.

Table 6
CPU times (s) for clusters at different clustering number N for Case 6.

N	Total									Max.	Min.	Ave.
1	35658.79841											
2	4627.708055	4199.952252	421.175725							4199.952252	421.175725	2310.563989
4	1444.509509	881.356017	205.015734	186.602952	165.190546					881.356017	165.190546	359.5413123
8	1229.048646	95.69621	152.021022	223.654529	112.994413	101.913815	127.773558	115.278783	293.349254	293.349254	95.69621	152.835198
16	1426.498538	68.988243	69.019327	82.548198	89.518775	100.960711	88.552028	110.131483	70.334471	110.131483	68.988243	85.0066545
		80.029979	72.147735	71.572883	151.654559	103.434949	84.679633	98.248576	78.258389			

Table 7
Optimal clustering number N for mechanisms of different sizes (numbers of species).

Mechanism size	$\mathcal{O}(10)$	$\mathcal{O}(10^2)$	$\mathcal{O}(10^3)$
Optimal clustering number, N	2	4–8	8–16

weight matrix for chemical kinetics. Three hydrocarbon fuel/air ignition problems with an increasing dimension of the mechanism, up to 2115 species and 8157 reactions, are taken into consideration under varying initial conditions.

Computational efficiency and accuracy can be improved by choosing a proper number of clusters to split the large system. For the n-heptane mechanism, partition by 4 clusters of species leads to about 8 times speedup compared to the non-split VODE solver and 10–20 times speedup versus the explicit solver CHEMEQ2. For the n-hexadecane mechanism, partition by 8 clusters of species results in a speedup factor of around 40. Clustering by diffusion maps based on a given weight matrix outperforms the simple clustering according to species' index in the mechanism, in terms of predicting the correct ignition delay time and post-ignition equilibrium state. It implies that an optimal clustering for a certain mechanism is preferable not only for computational acceleration but also for higher accuracy. An optimal choice of clustering number N is suggested in Table 7 in relation with the dimension of the mechanism to consider.

With a specific clustering number, there is still room to improve the present species-clustered splitting scheme to further reduce splitting errors, e.g., the total mass conservation error at the ignition instant. Either a new definition of weight matrix or other optimal partition techniques in addition to diffusion maps are worth of further investigation. Taking advantage of the fast convergence of operator-splitting methods, it is also possible to use adaptive sub-cycling or time-stepping to achieve better accuracy. The above splitting so far considers the first-order Lie–Trotter scheme or the second-order Strang scheme, and extension to higher-order splitting schemes is straightforward. Adaptive variable clustering number might be another option. Also, a combination of the species-clustered splitting scheme and sparse matrix techniques to obtain additional efficiency gain is possible.

Acknowledgments

The financial support from the EU Marie Skłodowska-Curie Innovative Training Networks (ITN-ETN) (Project ID: 675528-IPPAD-H2020-MSCA-ITN-2015) for the first author is gratefully acknowledged. Xiangyu Y. Hu is also thankful for the partial support by National Natural Science Foundation of China (NSFC) (Grant No.: 11628206).

Appendix A. Clustering of species for the three involved mechanisms based on diffusion maps

For the GRI-Mech 3.0 mechanism of methane (CH_4), by setting $N = 2$, we have the diffusion maps based clustering as

$$C^2 = \{c_1, c_2, \ldots, c_{52}, c_{53}\} = \{2, 2, 2, 2, 2, 2, 2, 2, 2, 2, 2, 2, 2, 2, 2, 1, 1, 1, 1, 1, 1, 2, 2, 2, 2, 1, 1, 2, 2, 2, 1, 1, 1, 1, 1, 1, 1, 1, 1, 1, 2, 1, 1, 2, 2, 2, 1, 1, 2, 1, 1, 1, 1, 1\}, \tag{A.1}$$

where $c_i = 1$ or 2 means the ith species is clustered into subset 1 or 2.

For the n-heptane (n-C_7H_{16}) mechanism, by setting $N = 8$, we have

$$C^8 = \{c_1, c_2, \ldots, c_{560}, c_{561}\} = \{5, 5, 5, 5, 5, 5, 5, 5, 5, 1, 5, 5, 5, 5, 5, 1, 1, 5, 1, 1, 1, 6, 6, 1, 1, 6, 5, 6, 1, 6, 6, 5, 5, 5, 1, 5, 5, 1, 1, 1, 1, 1, 1, 1, 5, 1, 1, 1, 1, 1, 1, 5, 5, 5, 5, 5, 5, 6, 8, 8, 8, 8, 8, 8, 8, 8, 1, 5, 8, 8, 1, 1, 1, 5, 1, 5, 1, 6, 6, 6, 6, 4, 1, 6, 6, 1, 1, 4, 4, 4, 4, 4, 4, 1, 1, 1, 1, 1, 1, 6, 6, 5, 4, 1, 1, 7, 8, 7, 3, 2, 4, 2, 4, 4, 4, 2, 4, 4, 2, 4, 2, 4, 2, 4, 4, 4, 4, 6, 6, 6, 6, 6, 1, 1, 1, 1, 1, 1, 1, 1, 1, 1, 1, 1, 8, 8, 3, 3, 6, 8, 8, 8, 8, 8, 8, 8, 8, 8, 8, 8, 8, 4, 2, 4, 2, 4, 2, 4, 4, 2, 2, 2, 2, 2, 4, 2, 4, 2, 2, 2, 2, 4, 4, 2, 2, 4, 2, 1, 6, 7, 7, 6, 6, 6, 5, 5, 5, 3, 3, 3, 5, 5, 5, 2, 4, 2, 2, 2, 2, 4, 2, 2, 4, 2, 4, 2, 2, 4, 2, 4, 2, 4, 4, 1, 7, 7, 6, 1, 7, 8, 3, 8, 8, 4, 6, 1, 5, 5, 6, 6, 6, 8, 5, 3, 1, 7, 7, 7, 7, 7, 7, 7, 7, 7, 7, 6, 8, 7, 7, 7, 7, 7, 7, 7, 7, 7, 7, 3, 6, 7, 3, 3, 7, 3, 7, 7, 3, 6, 7, 4, 5, 5, 6, 5, 6, 5, 5, 1, 5, 6, 6, 6, 4, 6, 8, 3, 8, 3, 8, 4, 4, 6, 6, 5, 5, 5, 5, 6, 8, 5, 8, 8, 5, 5, 5, 6, 7, 1, 5, 6, 6, 3, 6, 5, 6, 6, 6, 5, 6, 5, 8, 5, 6, 3, 6, 6, 3, 5, 7, 7, 3, 3, 8, 3, 3, 6, 5, 3, 3, 3, 3, 3, 5, 3, 3, 3, 3, 8, 3, 3, 5, 3, 3, 3, 5, 6, 6, 6, 6, 3, 3, 3, 3, 6, 3, 6, 6, 6, 1, 8, 8, 8, 1, 6, 6, 6, 1, 7, 7, 7, 1, 7, 6, 6, 8, 8, 8, 5, 8, 8, 2, 4, 2, 2, 2, 2, 4, 2, 2, 4, 2, 2, 4, 2, 2, 4, 2, 2, 4, 4, 4, 2, 2, 4, 4, 4, 4, 2, 3, 7, 7, 7, 7, 7, 7, 7, 3, 7, 7, 7, 7, 7, 8, 8, 8, 8, 8, 8, 8, 8, 1, 1, 1, 8, 8, 8, 8, 8, 8, 8, 8, 8, 8, 8, 8, 8, 8, 2, 4, 2, 2, 2, 2, 4, 4, 2, 4, 2, 2, 4, 2, 2, 2, 2, 4, 4, 2, 4, 4, 4, 4, 2, 2, 2, 4, 4, 1, 6, 7, 7, 1, 7, 7, 7, 1, 6, 3, 7, 7, 7, 3, 7, 7, 7, 7, 3, 7, 7, 7, 7, 3, 3, 7, 7, 5, 6, 3, 3, 3, 3, 3, 5, 3, 3, 3, 5, 3, 3, 3, 3, 3, 3, 3, 3, 3, 3, 3, 3, 3, 3, 3, 8, 7, 5\}. \tag{A.2}$$

For the n-hexadecane (n-$C_{16}H_{34}$) mechanism, by setting $N = 8$, we have

$$C^8 = \{c_1, c_2, \ldots, c_{2114}, c_{2115}\} = \{3773373111111111181111111111111111117115575 7533337311117771133555536563555775377767773535 3577777755777777557757577777775777555777777187 7735335333777777777755561226612216612288822888 8822881414111111111555353335335355557777555566 6266652166612116244822488822488842777777777714 4411414111111141557777757775577771117111711753 3333333333333333333333335555555555555555555555 5355555355555355553333333333333333333333555575 5377775377753777537353333333333333333333333333 3555555555555555555555555555555555333333333333 3333333333355555555555555555555555555555555533 3333333333333333333335555555555555555555777777 7777777766886668866668886668888666688886668688 8866668888666688662266622666622266662222666622 2266662222666622226666226662266662226666222266 6622226666222266662266886668866668886666888866 6688886666888866662266622666622216662222666622 2266662266226662266662226666222266662222666122 6612216612221661222216612261226612216612221661 2222166122661221661222166122888888888888888888 8888888888888888888888888888888888882222222222 2222222222222222242222222422222224222242222822 2282222882222488822224888842248888422888888888 8888888888888888888888888888888888822882228822 2488882248888422488884224882288224888224888224 8888422488884228882248882248884224888842288828 8224888224888422488884228882248882248884228887 7677677776776677667767767777677777776776677667 7667677767767776677667766776777677667766776677 6676777677667766776777677667766776677667677767 7667776776777776777777676777677677671114111141 1114411114441111444411414444144444444444444114 4111141111441114444111144441144444414444444444 1144111441114441114444111144441144444414444444 1441144411144411144441114444411444444444414411 4441114441114444111444444144444414441144411144 1114444144444444444144114441114441414444444444 4414441144411144414144444444144411441114141414 4443355555553355555557555555561755555551115555 5333355377333333333}, \tag{A.3}$$

leaving out the delimiter.

References

[1] I.E. Mersin, E.S. Blurock, H.S. Soyhan, A.A. Konnov, Hexadecane mechanisms: comparison of hand-generated and automatically generated with pathways, Fuel 115 (2014) 132–144, doi:10.1016/j.fuel.2013.06.055.

[2] O. Herbinet, W.J. Pitz, C.K. Westbrook, Detailed chemical kinetic oxidation mechanism for a biodiesel surrogate, Combust. Flame 154 (3) (2008) 507–528.

[3] T. Lu, C.K. Law, Toward accommodating realistic fuel chemistry in large-scale computations, Progr. Energy Combust. Sci. 35 (2) (2009) 192–215, doi:10.1016/j.pecs.2008.10.002.

[4] C. Xu, Y. Gao, Z. Ren, T. Lu, A sparse stiff chemistry solver based on dynamic adaptive integration for efficient combustion simulations, Combust. Flame 172 (2016) 183–193.
[5] T. Lu, C.K. Law, A directed relation graph method for mechanism reduction, Proc. Combust. Inst. 30 (1) (2005) 1333–1341.
[6] P. Pepiot-Desjardins, H. Pitsch, An efficient error-propagation-based reduction method for large chemical kinetic mechanisms, Combust. Flame 154 (1) (2008) 67–81, doi:10.1016/j.combustflame.2007.10.020.
[7] W. Sun, Z. Chen, X. Gou, Y. Ju, A path flux analysis method for the reduction of detailed chemical kinetic mechanisms, Combust. Flame 157 (7) (2010) 1298–1307, doi:10.1016/j.combustflame.2010.03.006.
[8] K.E. Niemeyer, C.-J. Sung, M.P. Raju, Skeletal mechanism generation for surrogate fuels using directed relation graph with error propagation and sensitivity analysis, Combust. Flame 157 (9) (2010) 1760–1770, doi:10.1016/j.combustflame.2009.12.022.
[9] P.N. Brown, G.D. Byrne, A.C. Hindmarsh, VODE: a variable-coefficient ode solver, SIAM J. Sci. Stat. Comput. 10 (5) (1989) 1038–1051.
[10] M. Caracotsios, W.E. Stewart, Sensitivity analysis of initial value problems with mixed odes and algebraic equations, Comput. Chem. Eng. 9 (4) (1985) 359–365, doi:10.1016/0098-1354(85)85014-6.
[11] Y. Morii, H. Terashima, M. Koshi, T. Shimizu, E. Shima, ERENA: a fast and robust jacobian-free integration method for ordinary differential equations of chemical kinetics, J. Comput. Phys. 322 (2016) 547–558.
[12] F. Perini, E. Galligani, R.D. Reitz, A study of direct and Krylov iterative sparse solver techniques to approach linear scaling of the integration of chemical kinetics with detailed combustion mechanisms, Combust. Flame 161 (5) (2014) 1180–1195.
[13] V. Damian, A. Sandu, M. Damian, F. Potra, G.R. Carmichael, The kinetic preprocessor KPP – a software environment for solving chemical kinetics, Comput. Chem. Eng. 26 (11) (2002) 1567–1579.
[14] Z. Ren, C. Xu, T. Lu, M.A. Singer, Dynamic adaptive chemistry with operator splitting schemes for reactive flow simulations, J. Comput. Phys. 263 (2014) 19–36.
[15] M. Singer, S. Pope, Exploiting ISAT to solve the reaction–diffusion equation, Combust. Theory Model. 8 (2) (2004) 361–383.
[16] M. Singer, S. Pope, H. Najm, Operator-splitting with ISAT to model reacting flow with detailed chemistry, Combust. Theory Model. 10 (2) (2006) 199–217.
[17] O.M. Knio, H.N. Najm, P.S. Wyckoff, A semi-implicit numerical scheme for reacting flow: II. Stiff, operator-split formulation, J. Comput. Phys. 154 (2) (1999) 428–467.
[18] Z. Ren, S.B. Pope, Second-order splitting schemes for a class of reactive systems, J. Comput. Phys. 227 (17) (2008) 8165–8176.
[19] Y. Gao, Y. Liu, Z. Ren, T. Lu, A dynamic adaptive method for hybrid integration of stiff chemistry, Combust. Flame 162 (2) (2015) 287–295.
[20] K. Nguyen, A. Caboussat, D. Dabdub, Mass conservative, positive definite integrator for atmospheric chemical dynamics, Atmos. Environ. 43 (40) (2009) 6287–6295.
[21] S. Pan, J. Wang, X. Hu, N.A. Adams, A network partition method for solving large-scale complex nonlinear processes, 2018, arXiv preprint arXiv:1801.06207.
[22] R.R. Coifman, S. Lafon, Diffusion maps, Appl. Comput. Harmon. Anal. 21 (1) (2006) 5–30.
[23] S. Lafon, A.B. Lee, Diffusion maps and coarse-graining: a unified framework for dimensionality reduction, graph partitioning, and data set parameterization, IEEE Trans. Pattern Anal. Mach. Intell. 28 (9) (2006) 1393–1403.
[24] R.R. Coifman, S. Lafon, A.B. Lee, M. Maggioni, B. Nadler, F. Warner, S.W. Zucker, Geometric diffusions as a tool for harmonic analysis and structure definition of data: diffusion maps, Proc. Natl. Acad. Sci. U.S.A. 102 (21) (2005) 7426–7431.
[25] M.I. Malinen, P. Fränti, Balanced k-means for clustering, 2014 Joint IAPR International Workshops on Statistical Techniques in Pattern Recognition (SPR) and Structural and Syntactic Pattern Recognition (SSPR), Springer (2014), pp. 32–41.
[26] R.I. McLachlan, G.R.W. Quispel, Splitting methods, Acta Numer. 11 (2002) 341–434.
[27] G. Strang, On the construction and comparison of difference schemes, SIAM J. Numer. Anal. 5 (3) (1968) 506–517.
[28] D.A. Schwer, J.E. Tolsma, W.H. Green Jr., P.I. Barton, On upgrading the numerics in combustion chemistry codes, Combust. Flame 128 (3) (2002) 270–291.
[29] M. Domijan, What are... some graphs of chemical reaction networks?, Vol. 1, Mathematics Institute, University of Warwick, Coventry CV4 7AL, United Kingdom (2008), pp. 1–18.
[30] MATLAB, MATLAB Version 9.1.0.441655 (R2016b), The MathWorks Inc., Natick, Massachusetts, 2016.
[31] D.R. Mott, E.S. Oran, CHEMEQ2: a solver for the stiff ordinary differential equations of chemical kinetics, Technical Report, Naval Research Lab Washington DC, 2001.
[32] J.-H. Wang, S. Pan, X.Y. Hu, N.A. Adams, A split random time-stepping method for stiff and nonstiff detonation capturing, Combust. Flame (2018), doi:10.1016/j.combustflame.2019.03.0.
[33] G.P. Smith, D.M. Golden, M. Frenklach, N.W. Moriarty, B. Eiteneer, M. Goldenberg, C.T. Bowman, R.K. Hanson, S. Song, W.C. Gardiner Jr., et al., Gri 3.0 mechanism, 21, Gas Research Institute, Des Plaines, IL (1999), p. 2017. accessed Aug
[34] H.J. Curran, P. Gaffuri, W.J. Pitz, C.K. Westbrook, A comprehensive modeling study of n-heptane oxidation, Combust. Flame 114 (1–2) (1998) 149–177.
[35] H.J. Curran, P. Gaffuri, W.J. Pitz, C.K. Westbrook, A comprehensive modeling study of iso-octane oxidation, Combust. Flame 129 (3) (2002) 253–280.
[36] C. Westbrook, W. Pitz, O. Herbinet, E. Silke, H. Curran, A detailed chemical kinetic reaction mechanism for n-alkane hydrocarbons from n-octane to n-hexadecane, Technical Report, Lawrence Livermore National Laboratory (LLNL), Livermore, CA, 2007.
[37] D.J. Seery, C.T. Bowman, An experimental and analytical study of methane oxidation behind shock waves, Combust. Flame 14 (1) (1970) 37–47.
[38] C.S. Yoo, T. Lu, J.H. Chen, C.K. Law, Direct numerical simulations of ignition of a lean n-heptane/air mixture with temperature inhomogeneities at constant volume: parametric study, Combust. Flame 158 (9) (2011) 1727–1741.
[39] C.K. Westbrook, W.J. Pitz, O. Herbinet, H.J. Curran, E.J. Silke, A comprehensive detailed chemical kinetic reaction mechanism for combustion of n-alkane hydrocarbons from n-octane to n-hexadecane, Combust. Flame 156 (1) (2009) 181–199.